Journal of Archaeological Science 53 (2015) 49–60

Contents lists available at ScienceDirect

Journal of Archaeological Science

journal homepage: http://www.elsevier.com/locate/jas

Technological tradition of the Mongol Empire as inferred from bloomery and cast iron objects excavated in Karakorum

Jang-Sik Park [a, *], Susanne Reichert [b, 1]

[a] Department of Metallurgical Engineering, Hongik University, 2639 Sejong-ro, Jochiwon, Sejong 339-701, Republic of Korea
[b] Rheinische Friedrich-Wilhelms-Universität Bonn, Vor- und Frühgeschichtliche Archäologie, Regina-Pacis-Weg 7, 53113 Bonn, Germany

ARTICLE INFO

Article history:
Received 22 May 2014
Received in revised form
1 October 2014
Accepted 4 October 2014
Available online 12 October 2014

Keywords:
Mongol Empire
Karakorum
Iron tradition
Bloomery iron
Cast iron
Steelmaking

ABSTRACT

Iron objects from Karakorum, the former capital of the Mongol Empire, were metallographically examined. Most were forged out of bloomery iron, particularly those requiring superior functional properties. By contrast, approximately one third were made from cast iron, with carbon levels approximating either cast iron or ultrahigh carbon steel. The carbon concentration of the bloomery products was controlled either by a carburization treatment directed at the functional parts or by the welding of a pre-carburized steel plate to a low carbon body. By comparison, cast iron-based steelmaking was achieved by subjecting pieces of solid cast iron to a combined thermal and mechanical treatment aimed at accelerating decarburization. Some anonymous cast objects were circulated as a feedstock for this unique process, naturally taking the form of thin plates. Also, the cast products examined were contaminated with substantial amounts of sulfur and silicon, suggesting that they originated from liquid iron smelted at relatively high temperatures using fossil fuel instead of charcoal. Given these findings, it can be concluded that the Mongol Empire took advantage of an effective multi-faceted iron tradition, which combined bloomery-based and cast iron-based iron technologies. It is important to note, however, that the former still remained the key technological tradition dominating the local contemporary iron industry.

1. Introduction

From their microscopic examination of a number of iron artefacts recovered at Xiongnu sites in Mongolia, Park et al. (2010) found that the use of bloomery iron and steel making through carburization formed the basis of the Xiongnu iron industry. This result was unexpected, given scholarly emphasis on relations of political and economic dependency between the Xiongnu Empire (209 BC–AD 155) in Mongolia and the Han Dynasty (206 BC–AD 220) in China (Barfield, 2001; Kradin, 2002), but is in line with the theory viewing Chinese influence as less critical for the Xiongnu development (Honeychurch, 2013, 2014). By the beginning of the Han period, China had established a mature iron industry based on the smelting of cast iron and a variety of steelmaking processes involving cast iron (Needham, 1980; Rostoker and Bronson, 1990; Wagner, 2008). Cast iron objects were also used in Mongolia at the same time, but so far cast iron has only been identified in the making of wheel components for wagons (Gelegdorj et al., 2007). It is not clear, therefore, whether such cast iron implements were of domestic origin or imported.

It is of significance to note that the two neighboring ancient states, despite their rich cultural and political interactions, inherited iron traditions fundamentally different in technological as well as historical contexts (Rostoker and Bronson, 1990; Tylecote, 1962). This difference may reflect their dissimilar life styles; namely nomadic versus sedentary and small-scale iron production with a low initial investment versus mass production with a high initial investment. Other factors may include the particular infrastructures previously established and certain technological and economic constraints. One immediate inquiry raised by this difference concerns the later development of iron traditions in both regions with the passage of time. The fact that the modern iron industry is based on the smelting of cast iron while bloomery technology is no longer practiced may lead one to presume that the iron tradition in Mongolia progressed from bloomery-based to cast iron-based due to an increase in Chinese influence. This hypothesis, which concerns technological development in Mongolia, may be viewed in a much wider context if the achievement made by the

* Corresponding author. Tel.: +82 44 860 2562; fax: +82 44 866 8493.
E-mail addresses: jskpark@hongik.ac.kr (J.-S. Park), susanne.reichert@uni-bonn.de (S. Reichert).
[1] Tel.: +49 0 228 73 6378.

http://dx.doi.org/10.1016/j.jas.2014.10.005
0305-4403/

Mongol Empire, particularly in its territorial expansion, is taken into account. It is important to note that the Mongol conquest encompassing China, Iran, Central Asia and much of the Near East and Russia provided the most significant early connection between East and West, bringing Europe in direct contact with Asia. This connection may be considered an early phase of the globalization in which exchange of material and human resources was greatly promoted throughout the empire (Fitzhugh, 2013: 23; Honeychurch, 2010: 415). The increased contacts and flow of cultural and technological ideas must have had impacts on the evolution of iron technologies in various geographical regions under the Mongol governance. This possibility is even more likely, given that Mongol rulers were predisposed to moving crafts people and their technologies between regions within the empire as a form of a gift-giving between elites (Allsen, 2002). The above hypothesis on Mongolian iron technology, therefore, concerns an important aspect not only of Mongolian history but also of world history, which can only be tested when the changing role of bloomery iron and cast iron in Mongolia is properly evaluated in terms of their production and use in iron and steel making.

In this respect, the research conducted by the Mongol–Japanese joint expedition (Amartuvshin et al., 2012) is particularly notable as it produced evidence of bloomery smelting practiced within the Mongolian territory during the Xiongnu period. As for the Mongol period, strong evidence of finery and forging was found at Avraga, a settlement site in the Delgerkhaan Sum, Khentii Province (Shiraishi and Tsogtbaatar, 2009; Sasada and Ishtseren, 2012). In addition, Ernst Pohl of Bonn University (Pohl et al., 2012) is currently excavating a Mongol period settlement area west of Karakorum on the western terrace of the Orkhon River. This excavation, conducted in cooperation with the Archaeological Institute of the Mongolian Academy of Sciences, produced promising preliminary results on iron technology. Evidence of smelting practiced in Mongolia, however, is still inconclusive. This is particularly true for the smelting of cast iron for which no convincing archaeological material has yet been reported.

Nevertheless, cast iron objects continued to be used in Mongolia from the Xiongnu period onwards. Both written and material evidence (Perlee, 1959, 1961) attest to this fact and suggest that its use was greatly promoted during the Khitan period (10th to 12th century AD). Thus, one may expect that this Khitan tradition was more or less carried forward to the Mongol Empire (13th to 15th century AD). In their study on cast iron artefacts recovered from certain Khitan and Mongol sites, Park et al. (2008) discovered a notable transition in cast iron technology brought about by the use of mineral coal, instead of wood charcoal, in smelting. They concluded that the transition began during the Khitan period and was inherited by the Mongol Empire. Given these findings, such a transition reflects an increased demand for cast iron at the time, which likely had a significant impact on Mongolian iron production. Cast iron in as-smelted conditions, however, has only limited applicability because of its inferior mechanical properties. As such, the real motivation for the production and circulation of cast iron lies in the expectation that it can be made into more versatile materials with better functional properties such as iron and steel. Evidence for the practice of iron and steel making from cast iron, therefore, is critical for determining the extent to which cast iron made a contribution, if any, to the traditions and transitions in Mongolian iron technology.

Despite the great success of the Mongol Empire in bringing most of the Eurasian landmass under its control, little is known of the technological environment surrounding the empire before and after its establishment. This lack of information is particularly pronounced in assessing the iron-production technology used despite its critical role in the warfare and achievements of this empire. In light of this concern, numerous iron objects from the Mongolian–German collaborative expedition at Karakorum (Fig. 1), the capital of the Mongol Empire until it was relocated to Shang-tu in 1260, serve as an invaluable archaeological assemblage that may provide clues for assessing the local iron industry at the time. Since current data is quite limited, the first objective of this work is to characterize these individual iron objects in terms of raw materials, steelmaking and various thermo–mechanical treatments applied during fabrication. The results will then be compared to test the hypothesis proposed above regarding the role of bloomery-based and cast iron-based technologies in the evolution of Mongolian iron traditions up to the Mongol period.

2. Comments on site and artefacts

All the objects presented in this paper came from the excavations conducted by Bonn University in the city center of Karakorum from 2000 to 2005 (Fig. 1), under the Mongolian-German-Karakorum-Expedition project. Directly south of the main cross-road remains of workshops were uncovered which may be linked to the Cathay, i.e. Chinese, according to William of Rubruck, a Franciscan monk who visited the city in 1254 (Jackson, 1990).

The selection of objects for analysis was based on several criteria: (1) The finds should be identifiable in order to gain transferrable technological insights; (2) they should represent a wide range of different artefact categories; (3) they should cover the complete stratigraphical sequence, preferably from several parts of the excavation.

Stratigraphical data on the objects are summarized in Table 1 and follow the local grid of 1-m-squares used during the excavation (Pohl, 2009: 64–68). In addition, the finds were attributed to the three main settlement periods as characterized by Pohl (2009: 126–134). The first and earliest settlement period (I) saw the construction of the main road and the initial occupation of the areas east and west of the street in the 1230s and 1240s AD. East of the street, especially, there are features such as walled furnaces and wooden trunks for foundations of anvils that attest to the use of the buildings as handicraft workshops. In the second period, dating to the second half of the 13th century, the main street was further developed by adding two drainage ditches along the road while buildings east and west of the street were renewed. Throughout the third period, dating approximately to the 14th century, maintenance of the street deteriorated although there were still new building activities on top of the older remains. At this stage it would be highly speculative to attribute any of the building layers to factual historical dates such as the transference of the capital status in 1260. However, the three main phases of occupation serve as an initial sequence of development in the city center.

Fig. 2 illustrates the general appearance of the objects examined, with the arrows indicating the spots from which specimens were taken for examination. Here, the bar under the number labeling each object corresponds to 1 cm. Table 1 provides summary information on the functions of the artefacts as inferred from their appearance and exact recovery spots. In addition, a brief description of the microstructure, chemical composition and fabrication method for each artefact is provided. The methods employed for the determination of this analytical data are described in the next section. The numbers labeling the objects are consistent in Table 1 and Fig. 2. The objects in Fig. 2 are mostly finished products and their intended function can be inferred from their appearance. One exception to this is found in a group of objects (#21–24) that are similar in shape and take the form of rectangular rods with a near-square cross section. They were also found at other sites of the Mongol period, frequently in large amounts (Pohl et al., 2012: 53; Shiraishi and Tsogtbaatar, 2009: 559). It is often speculated that

Fig. 1. Physical map of Mongolia. The arrow indicates the site at Karakorum, the former capital of the Mongol Empire, in the Ovorkhangai province from which the iron objects examined in this work were recovered.

they were used as product intermediaries for further processing (Osawa, 2005: 45).

3. Laboratory examination and results

Specimens were taken from the iron objects in Fig. 2 for microscopic examination. The specimens were mounted and polished following the standard metallographic procedures of grinding and polishing, and then etched with a solution of 2 volume % nitric acid in methanol. Their etched microstructures were subsequently examined using an optical microscope and a scanning electron microscope (SEM). Their chemistry was assessed using the energy dispersive X-ray spectrometer (EDS) included with the SEM instrument. The relevant numerical data are reported in Table 1 according to weight fraction.

All the specimens taken from objects #1 through #11 in Fig. 2 were similarly made of almost pure iron containing profuse nonmetallic inclusions. Some of them were found to include areas filled with pearlite. The carbon content as inferred from the fraction of pearlite, however, was mostly well below 0.1%, which is not high enough to have a notable effect on the material properties of the objects. More importantly, the distribution pattern of pearlite showed no evidence of its presence intended for a specific purpose. A typical structure representing these specimens is presented in Fig. 3a, an optical micrograph showing the structure at the rear end (arrow b) of object #4. Fig. 3a consists predominantly of ferrite grains forming the background where the dark non-metallic inclusions are scattered. Fig. 3b, a secondary electron image (SEI) micrograph magnifying the area near the arrow in Fig. 3a, reveals numerous tiny particles present inside the inclusions. Fig. 3c, an EDS spectrum taken from inside a ferrite grain at arrow 1 in Fig. 3b, detected no elements other than iron (Fe) and carbon (C). The ferrite grains in Fig. 3b correspond to almost pure iron, and the intensity of carbon in Fig. 3c must have been exaggerated due likely to the carbon atoms residing in the SEM chamber. It should be noted that the absence of such elements as silicon (Si) and phosphorous (P) in the ferrite of this specimen will serve as an important clue in our discussion of the smelting technology applied for the production of raw materials. Fig. 3d, an EDS spectrum taken at arrow 2 of Fig. 3b, indicates that the particle is iron oxide containing a substantial amount of calcium (Ca) and silicon. The spectrum from the particle at arrow 3 was similar except that the peak intensity for calcium was reduced. It is important to point out that nonmetallic inclusions consisting of such iron oxide particles are frequently introduced during smelting and play a key role in assessing associated production technologies.

Fig. 4a illustrates the variation of structures along the vertical line drawn in the inset, which covers the entire cross section of the front end (arrow a) of object #12 in Fig. 2. It is seen that the pearlite structure near the surface at the left edge (i.e., the top of the inset) gradually turns into a mixture of pearlite and ferrite as one goes to the right and into the interior. This trend is reversed, however, as one goes from the center to the surface at the right edge (i.e., the bottom of the inset). This transition in microstructure, reflecting the variation in carbon levels, demonstrates that the carbon concentration is higher in the near-surface area than in the inner part. This carbon distribution is unique to carburization where pieces of iron are buried inside burning charcoal for a prolonged period so that carbon atoms may diffuse to the iron from its surface. Fig. 4b presents three micrographs from left to right, providing a magnified view of the areas surrounding the Vickers indentation marks at arrows 1, 2 and 3 in Fig. 4a, respectively. The hardness number, as measured from the dark rhombuses in Fig. 4b, is approximately 210, 120 and 270 from left to right, in agreement with the expected carbon content. It is evident therefore that the carbon concentration of the front part of object #12 was raised through a carburization treatment. By contrast Fig. 4c, which shows the structure at the rear end of the object, is composed primarily of ferrite grains, and may better represent the raw material supplied. It is to be noted that this specimen also contains nonmetallic inclusions in the dark areas. EDS analyses done on them produced similar results to those presented in Fig. 3c and d.

Fig. 4d illustrates the structural variation along the vertical line drawn in the inset, which covers the entire longitudinal section of object #14 in Fig. 2. Two layers are clearly shown to run horizontally from one end of the inset to the other. Part of the dark layer at the bottom is magnified on the left hand side of Fig. 4d where the structure consists of a dark pearlite background containing islands

Table 1
Summary information, including stratigraphical and microstructure data, for the iron objects examined from Karakorum, the former capital of the Mongol Empire in Mongolia. The numbers labeling the objects are consistent with those in Fig. 2.

No	ID	Artifact	Find spot	Layer	Feature	Settlement period	Specimen location	Microstructure	Comments
1	1387	Hook	LH 28/67	3	206	III	Body	Ferrite; inclusions	F[a]
2	1506	Arrowhead	LH 27/78	3	–	III	a-head	Ferrite; inclusions	F
							b-tale	Ferrite; inclusions	
3	1752	Bar	LH 27/79	8	–	II	Body	Ferrite; some pearlite; inclusions	F
4	1861a	Hammer	LH 16/85	2	328	III	a-front	Ferrite; some pearlite; inclusions	F
							b-rear	Ferrite; inclusions	
5	2480	Tool	LH 27/65	18	–	I	a-blade	Ferrite; inclusions	F
							b-flank	Ferrite; inclusions	
							c-socket	Ferrite; some pearlite; inclusions	
6	2733	Arrowhead	LH 28/22	15	–	II	a-tip	Ferrite; inclusions	F
							b-flank	Ferrite; some pearlite; inclusions	
							c-tail	Ferrite; some pearlite; inclusions	
7	3457	Arrowhead	LH 18/59	10[b]	827	III	Body	Ferrite; inclusions	F
8	3671	Arrowhead	LH 28/93	22	–	I	a-tip	Ferrite; some pearlite; inclusions	F
							b-tail	Ferrite; inclusions	
9	4016	Knife	LH26/84	14	–	I	a-blade	Ferrite; some pearlite; inclusions	F
							b-tang	Ferrite; inclusions	
10	4487	Arrowhead	LH 16/97	5[b]	1821	III	a-tip	ferrite; inclusions	F
							b-flank	Ferrite; some pearlite; inclusions	
							c-tail	Ferrite; inclusions	
11	4949	Horseshoe	LH 26/90	14	–	I	a-body b-body	Ferrite; inclusions	F
								Ferrite; inclusions	
12	13	Hammer	LH 26/84	0	–	III	a-front	Pearlite; some inclusions	F- carburized
							b-rear	Ferrite; inclusions	
13	1374	Scissors	LH 28/67	3	206	III	a-blade	Pearlite; ferrite; inclusions	F- carburized
							b-handle	Ferrite; inclusions	
14	1644	Hatchet	LH 17/64	1[b]	256	III	Cross section	Pearlite plate welded to ferrite plate	F-welded –quenched
15	2071	Knife	LH 28/79	10[b]	–	II	Cross section	Pearlite; some ferrite	F
16	4164	Hoe	LH28/67	21	1778	I	a-blade	Tempered martensite; ferrite; inclusions	F-quenched- tempered
							b-flank	Ferrite; some pearlite; inclusions	
							c-socket	Ferrite; inclusions	
17	1561	Bowl	LH 17/63	0	–	III	Body	Pearlite in dendrites; high P phase between dendrites; iron sulfide	C[c]; 1.0S,1.0P[d]
18	2811	Moldboard	LH 28/82	20	–	I	Blade	Pearlite in dendrites; cementite between dendrites; iron sulfide	C; 0.8Si,1.1S,0.6P[d]
19	2845	Plowshare	LH 27/71	14	–	I	Blade	Same as object#18	C; 0.8Si,1.1S,0.6P[d]
20	4887	Vessel	LH 16/97	7	–	II/III	Handle	Same as object#17	C; 0.3Si,1.4S,1.7P[d]
21	399a	Ingot	LH 26/34	2	–	III	Body	Same as object#18	C; 0.5Si,1.5S,0.4P[d]
22	1034b	Ingot	LH 88/91	2	–	III	Body	Same as object#18	C; 0.3Si,1.5S,0.4P[d]
23	1240a	Ingot	LH 26/61	1	–	III	Body	Same as object#18	C; 0.4Si,1.4S,0.4P[d]
24	4885	Ingot	LH 16/87	7	–	II/III	Body	Same as object#18	C; 0.4Si,1.5S,0.6P[d]
25	1861b	Knife	LH 16/85	2	328	III	a-blade	Pearlite; cementite plates or particles;	C-F-decarburized;
							b-tang	elongated iron sulfide ribbons	0.3Si,0.3S,0.2P[d]
26	3151	Knife	LH28/43	17	–	II	a-blade	Pearlite; cementite plates or particles;	C-F-decarburized; 0.24Si[d]
							b-tip	elongated iron sulfide ribbons; blade hardened	
							c-back		
							d-tang		

[a] F = forged.
[b] Level instead of layer.
[c] C = cast.
[d] Chemistry based on weight fraction [%].

of martensite. This mixed structure of pearlite and martensite indicates that the specific part was cooled rapidly, though not at such a high rate as to suppress the precipitation of pearlite completely. It was found that the structure is fully martensitic only near the blade, indicating that the quenching was applied mainly for the hardening of the blade. By contrast, the white area shown on the right hand side of Fig. 4d is mostly filled with ferrite. The line running vertically at arrow A in Fig. 4d, which is a trace often left behind after welding, indicates that the object was fabricated by joining two iron plates. The concentration gradient evident in the area to the left of this line is an unmistakable sign of carburization although it is not immediately certain whether this was given before or after welding. The distinctive microstructural difference identified between the upper and lower layers throughout the entire section shown in the inset, however, suggests that the high carbon plate was first carburized for the subsequent assemblage. Otherwise, no structural discontinuity, such as the line clearly visible at arrow A in Fig. 4d, would have survived the full homogenization caused by the lengthy heating process for carburization. Fig. 4e presents five optical micrographs from left to right, each enlarging the vicinity of the Vickers hardness marks at arrows 1–5 in Fig. 4d, respectively. The hardness is approximately 800 in the martensite phase of the first two micrographs from the left, 350 in the dark pearlite structure below the martensite area of the second micrograph (see the indentation mark at the white arrow) and 160, 150 and 110 in the low carbon areas of the third to fifth micrographs, respectively. Nonmetallic inclusions are also seen in this specimen at the arrows labeled B in Fig. 4d. EDS analyses on the iron phases of this specimen detected no elements other than iron and carbon.

Fig. 4f shows the structure at the blade (arrow a) of object #16 in Fig. 2. The contrast between the upper and lower parts of Fig. 4f reflects the difference in microstructures. Fig. 4g presents two optical micrographs, one on the top and another on the bottom, which magnify the area near the Vickers marks at the upper and middle

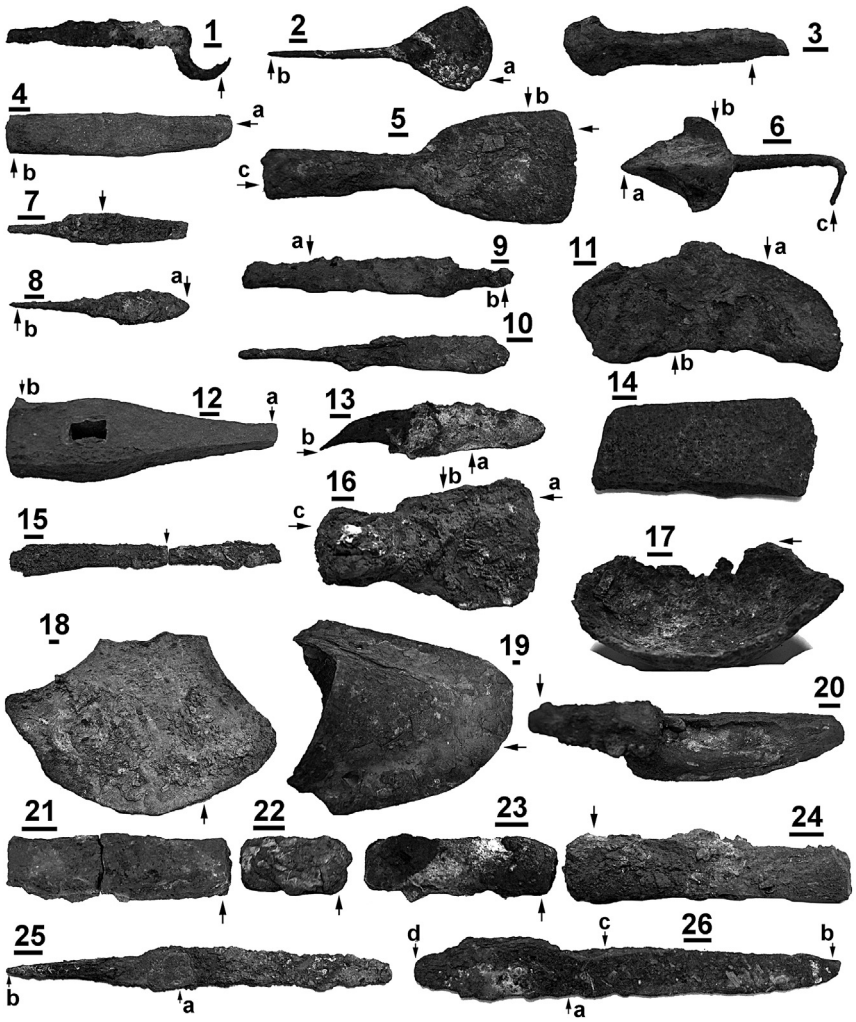

Fig. 2. The general appearance of the iron objects examined. Objects #1–16, 25 and 26 were forged to shape and objects #17–24 were cast to shape. The numbers labeling the objects are consistent with those in Table 1; the bars under the object numbers correspond to 1 cm.

parts of Fig. 4f, respectively. The top micrograph consists of fine ferrite grains, the hardness of which as determined from the rhombuses is estimated to be 160. The structure in the bottom micrograph looks fairly uniform and comprises micro-scale needles. Such a unique structure is obtained in a steel specimen when it is tempered after being quenched. The rhombuses in this bottom micrograph correspond approximately to a Vickers hardness of 220, suggesting that the specimen was given a substantial annealing treatment.

Fig. 5a, illustrating the structure at the arrow of object #24 in Fig. 2, retains the morphological characteristics of the solidification reaction. It is evident, therefore, that the object was cast to shape without any notable mechanical working subsequently applied. Here, the dark regions are covered with pearlite while the narrow bright areas in their boundaries represent the cementite phase. The carbon content inferred from the relative fraction of pearlite and cementite is 2% or less. Careful examination of Fig. 5a reveals a number of fine inclusions located primarily at the boundary regions. One of them, marked by the arrow, is better illustrated at arrow 1 in Fig. 5b, which enlarges the area surrounding the inclusion. Fig. 5c, an EDS spectrum taken from this inclusion, shows that it is an iron sulfide particle contaminated with trace amounts of copper (Cu) and manganese (Mn). Fig. 5d, an EDS spectrum from the small ferrite area at arrow 2 in Fig. 5b, contains a slight peak for silicon (Si), which corresponds approximately to 0.6% silicon included as a solute in the ferrite phase. It was found from the EDS analysis covering the entire area of Fig. 5a that the specimen contains approximately 0.4% Si, 0.6% P and 1.5% S on average. It is important to note that this specimen is distinguished from those discussed above, both in alloy compositions and method of fabrication. Also, objects #18, 19, 21–24 in Fig. 2 were similar to this object and were all fabricated exclusively by casting using iron–carbon alloys containing noticeable amounts of silicon, phosphorous and sulfur.

Fig. 6a shows the structure at the rear end of object #20 in Fig. 2. The structural characteristics developed during solidification are well preserved in this micrograph, just like those observed in Fig. 5a. This implies that the object also was fabricated primarily by casting. In Fig. 6a, however, the pearlite areas are significantly diminished such that they are completely isolated by the boundary regions. Furthermore, no proeutectoid cementite phase is observed anywhere in the micrograph. The carbon concentration is apparently too low to induce the precipitation of such cementite. Instead, the EDS analysis covering the entire area of Fig. 6a confirmed that the alloy contains 1.7% P, 0.3% Si and 1.4% S. This increased phosphorous content may have compensated for the relatively low carbon level, allowing the alloy to be cast. Micro-constituents making up this high phosphorous alloy are better identified in

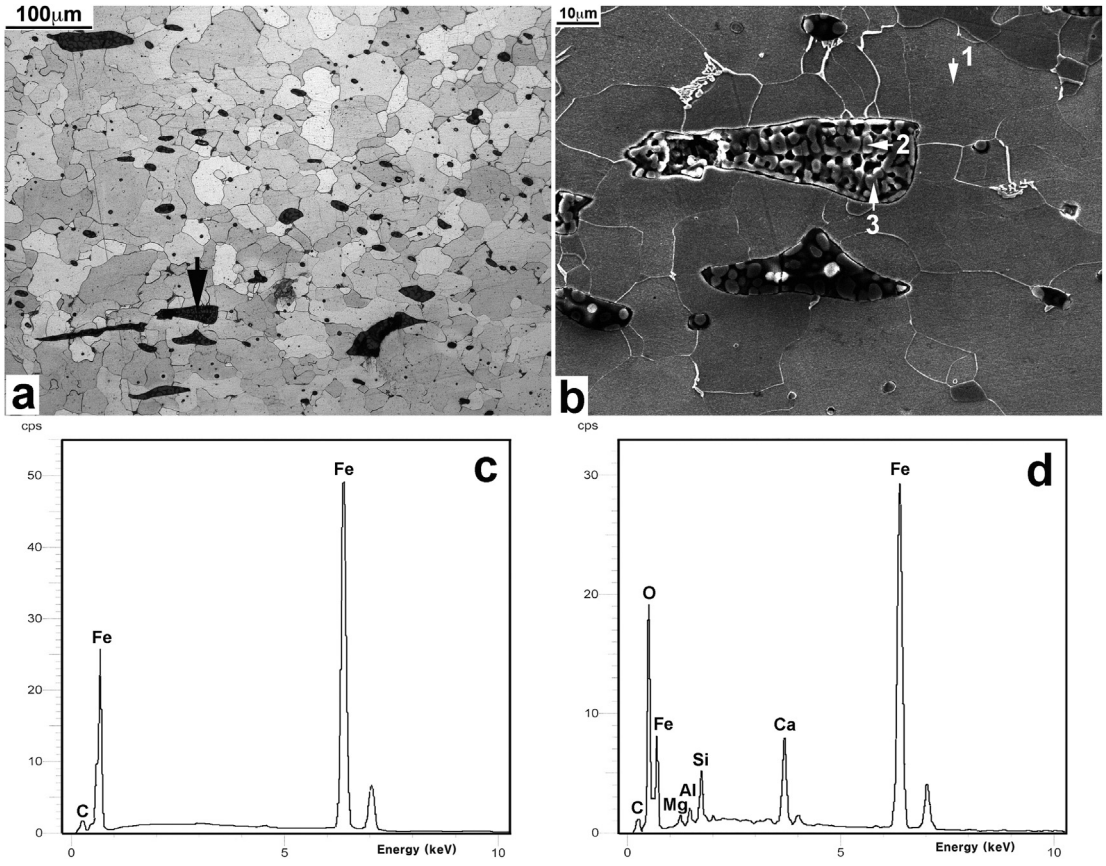

Fig. 3. Micrographs and EDS spectra. (a) Optical micrograph showing the structure of object #4 in Fig. 2 at arrow b, the rear end; (b) SEI micrograph enlarging the area marked by the arrow in (a); (c), (d) EDS spectra taken at arrows 1 and 2, respectively.

Fig. 6b, which enlarges the area marked by the arrow in Fig. 6a. In Fig. 6b, bright pearlite areas are observed near the left and right edges. During casting, such pearlite areas are precipitated first in the form of dendrites prior to the regions between them. Arrows 1, 2 and 3 in Fig. 6b indicate three different phases positioned between the two bright pearlite areas. It is inferred from Fig. 6c and d, EDS spectra taken at arrows 1 and 2, respectively, that the phase at arrow 1 contains approximately 0.3% Si and 0.8% P while that at arrow 2 contains 14.2% P. It is evident that the material at arrow 1 is the α phase while the particle at arrow 2 is the δ phase of the iron–phosphorous alloy system. The spectrum from arrow 3 was similar to that in Fig. 5c, indicating that this part is filled with iron sulfide. In Fig. 6b, the δ particles, precipitated along the former grain boundaries, apparently served as a sink for the excess phosphorous atoms rejected from the neighboring alpha areas upon cooling. No further nucleation of δ is, therefore, observed in their immediate neighborhood. By contrast, numerous events of δ-nucleation are verified in the bright two-phase region next to this single α area on either side of the boundary. Object #17 was similar to this object in terms of microstructures; however its phosphorous and sulfur levels were reduced to around 1.0% and its silicon content was below the detection limit of the EDS.

Fig. 7a shows the structure at the tang (arrow b) of object #25 in Fig. 2. In this low magnified micrograph, the bright spots seen in the interior away from the surfaces at the top and bottom represent particles of iron carbide. Their unique distribution pattern reveals two significant facts: First, the specimen was forged along the horizontal planes; second, there is more carbon in the inner space than near the surface. It is evident, therefore, that the specimen was decarburized while being forged. Fig. 7b, an optical micrograph, and Fig. 7c, a SEI micrograph, successively enlarging the area near the arrow in Fig. 7a, reveal features that are not visible in the low magnified micrograph. A number of tiny particles, elongated horizontally due to deformation, are seen in Fig. 7b, some of which are marked by the arrows. One of them at arrow 1 is greatly magnified and shown near the center of Fig. 7c at the arrow. An EDS spectrum of this particle can be seen in Fig. 7d. It shows that the particle contains iron sulfide with traces of titanium (Ti), vanadium (V) and manganese. It is similar in chemistry to the particle at arrow 1 in Fig. 5b, with a minor exception found only in the elements that exist in trace amounts. In the highly magnified micrograph of Fig. 7c, the general microstructure is clearly identified as consisting of numerous cementite particles in the pearlite matrix. The carbon concentration as inferred from this micrograph is well above 1%, indicating that object #25 was forged from ultrahigh carbon steel. It is important to note that the steel supplied was substantially contaminated with particles of iron sulfide.

Fig. 8a presents the structure at the back (arrow c) of the blade of object #26 in Fig. 2. Not much information on structural characteristics can be drawn from this low magnified micrograph. Nevertheless, the Vickers hardness is approximately 270, as measured from the two dark rhombuses, which reflect a carbon concentration that is not negligible. This is confirmed in Fig. 8b, which enlarges the area near the arrow in Fig. 8a. Fig. 8b shows a large presence of iron carbide, mostly in the form of spherical particles with a minor exception in lamellar form. The carbon concentration with this high level of carbide should be 1% or above. In such high-carbon alloys, it is difficult to avoid precipitating proeutectoid cementite. Moreover, the cementite phase is not generally precipitated in the form of particles as seen in Fig. 8b

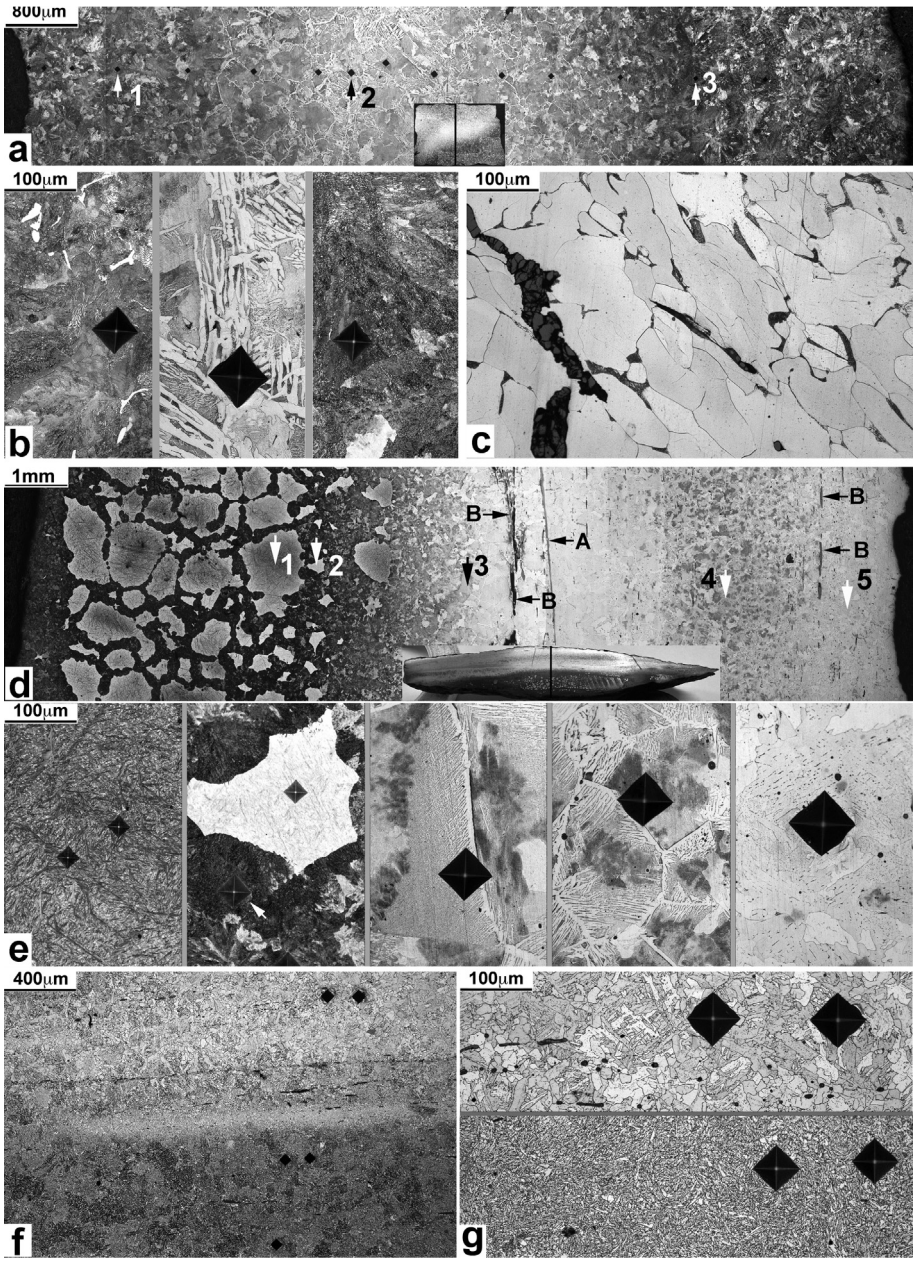

Fig. 4. Optical micrographs. (a) Micrograph showing the structure of object #12 in Fig. 2, along the vertical line drawn in the inset covering the entire cross section at arrow a; (b) 3 micrographs from left to right providing magnified views of the Vickers hardness marks at arrows 1, 2 and 3 in (a), respectively; (c) micrograph showing the structure at the rear end (arrow b) of object #12 in Fig. 2; (d) micrograph showing the structure of object #14 in Fig. 2, along the vertical line drawn in the inset covering the entire longitudinal section; (e) 5 micrographs from left to right enlarging the Vickers hardness marks at arrows 1–5 in (d), respectively; (f) micrograph showing the structure at the blade (arrow a) of object #16 in Fig. 2; (g) 2 micrographs from top to bottom magnifying the Vickers hardness marks at the upper and middle part of (f), respectively.

without special thermo–mechanical treatments. A clue as to the particular treatment given to this specimen can be found in Fig. 8a and b. Careful examination of Fig. 8a reveals the presence of numerous miniature areas appearing bright against the darker neighborhood. One of them at the arrow is magnified in Fig. 8b with its boundary outlined by the arrows. In this SEI micrograph, the outlined area is noticeably raised above its neighborhood. Evidently, the background within the boundary is not ferrite as would normally be expected in such steel specimens. Its higher elevation, therefore, suggests that it is martensite, which etches slower than ferrite and is typically raised above the neighboring ferrite area. This particular area, consisting of carbide particles in the background of martensite, reveals the occurrence of a unique phase transition referred to as divorced eutectoid transformation (DET) (Sherby et al., 1985). In the DET, cementite is precipitated in the form of spherical particles, unlike the lamellar structure in pearlite, across the austenite–ferrite boundary advancing toward the austenite area. The existence of martensite indicates that the specimen was quenched before the transition from austenite to ferrite was completed. The boundary depicted by the arrows in Fig. 8b represents the growth front of the DET that was frozen to form the current martensite–ferrite boundary. The DET technique, if combined with additional thermo–mechanical treatments, can effectively control the precipitation process of cementite in both the proeutectoid and eutectoid transformations for the desired shape and distribution of carbide. Evidence of the DET was also

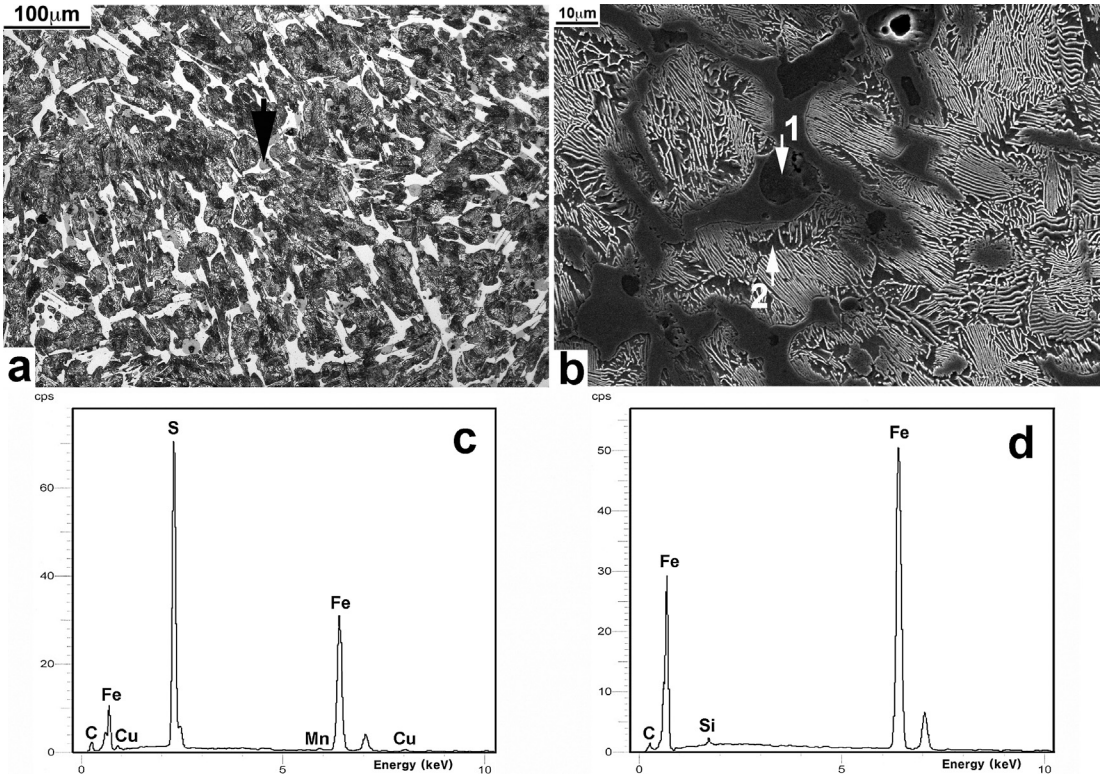

Fig. 5. Micrographs and EDS spectra. (a) Optical micrograph showing the structure at the arrow of object #24 in Fig. 2; (b) SEI micrograph enlarging the area marked by the arrow in (a); (c), (d) EDS spectra taken at arrow 1 and 2 in (b), respectively.

identified in the other specimens taken from object #26. The lamellar pearlite structure found in some parts of Fig. 8b, however, indicates that the control of carbide precipitation was not perfect. Fig. 8c, showing the structure at arrow b of object #26, illustrates another failed attempt where the proeutectoid cementite was precipitated in large-scale plates, instead of fine particles. An important effect of carbide morphology in ultrahigh carbon steel is illustrated in Fig. 8d, which shows the structure at arrow a of object #25. This micrograph visualizes, in the bright areas, fragmentation of large carbide particles upon forging and, at the arrows, particles of iron sulfide elongated horizontally along the forging planes. It is important to note that without the proper control of carbide precipitation, a similar fracture can occur upon receiving impact, leading to a premature failure.

4. Discussion

Table 1 summarizes the microstructure and fabrication method of the specimens examined, with the alloy compositions specified only for those containing minor elements in addition to iron and carbon. The objects are arranged in Table 1, and also in Fig. 2, based on the fabrication method as inferred from their microstructure. It is then immediately evident that they can be classified into four groups; the first group of objects #1–11, forged from almost pure iron; the second group of objects #12–16, forged from iron and steel; the third group of objects #17–24, cast to shape; and the fourth group of objects #25 and #26, forged from ultrahigh carbon steel. The members of the first two groups are distinguishable from those of the other groups in terms of overall alloy compositions as well as in the chemistry and distribution of nonmetallic inclusions. This difference is a strong indication that the raw materials supplied were derived from two distinctly different engineering processes, and is indicative of the two major smelting technologies, i.e., bloomery and cast iron, practiced widely in pre-industrial worlds.

It is seen in Table 1 that the members of the first two groups (objects #1–16) were all forged from low carbon iron containing a substantial amount of iron oxide-based inclusions. The major difference between these two groups lies in the relative fraction and distribution pattern of high carbon structures, pearlite and martensite. Certain areas of pearlite were frequently observed in some of the specimens belonging to the first group. No evidence was found, however, that they resulted from a controlled treatment intended for hardening. By contrast, objects in the second group contain pearlite or martensite at the specific parts where strength is a key requirement for functional purposes. The structural variations, as observed in Fig. 4a and d, reveal that the high carbon areas are preferentially located near the surface, portraying a reaction that occurred in the carburization treatment where carbon atoms were supplied from the surface. It is important to note that Fig. 4a and d represent two different example cases in the application of the carburization technique. The structural distribution in Fig. 4a demonstrates that the technique was applied after completion of the shaping, with its effect reaching most of the entire cross section. Such heavy carburization was likely meant to improve the overall load-bearing capacity or strength of the specific part (see arrow a in #12 of Fig. 2) rather than the surface hardness. By contrast, in a tool like object #14, only the limited part near the blade would need special strength or hardness. To this end, a carburization treatment is often applied exclusively to a specific part of a finished object. In this case, the effect is restricted to a thin layer near the blade. A similar treatment would have been needed whenever the hardened layer was worn out from use. This specific inconvenience is alluded to in a famed Biblical story (see Samuel 1 chapter 13) where the Israelites frequently had to visit the Philistines to have their

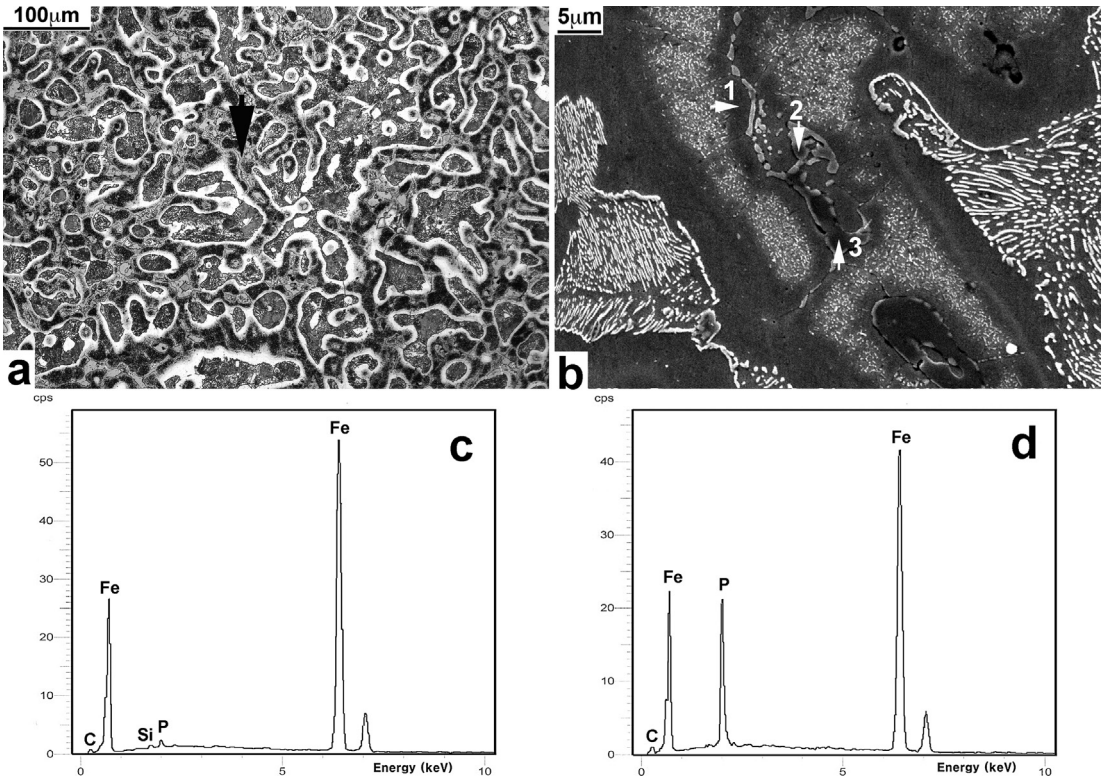

Fig. 6. Micrographs and EDS spectra. (a) Optical micrograph showing the structure at the arrow of object #20 in Fig. 2; (b) SEI micrograph enlarging the area marked by the arrow in (a); (c), (d) EDS spectra taken at arrows 1 and 2 in (b), respectively.

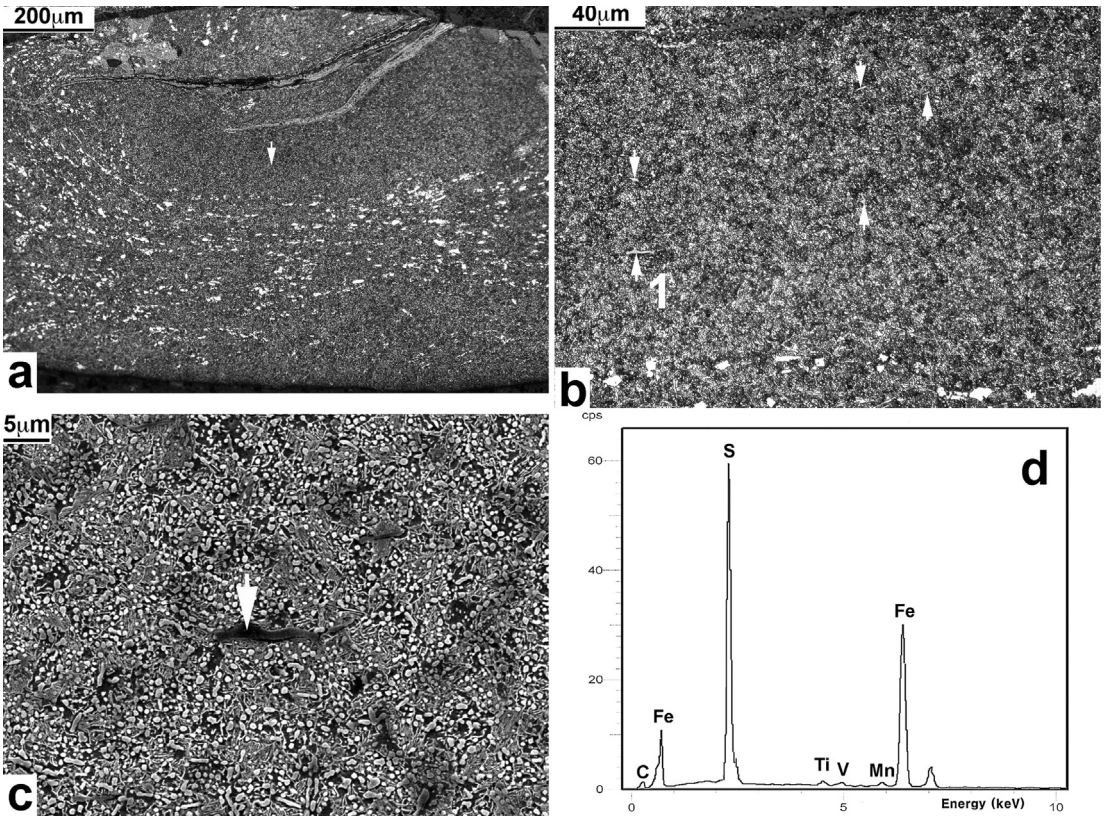

Fig. 7. Micrographs and EDS spectrum. (a) Optical micrograph showing the structure at the tang (arrow b) of object #25 in Fig. 2; (b) optical micrograph enlarging the area marked by the arrow in (a); (c) SEI micrograph enlarging the area marked by arrow 1 in (b); (d) EDS spectrum taken at the arrow in (c).

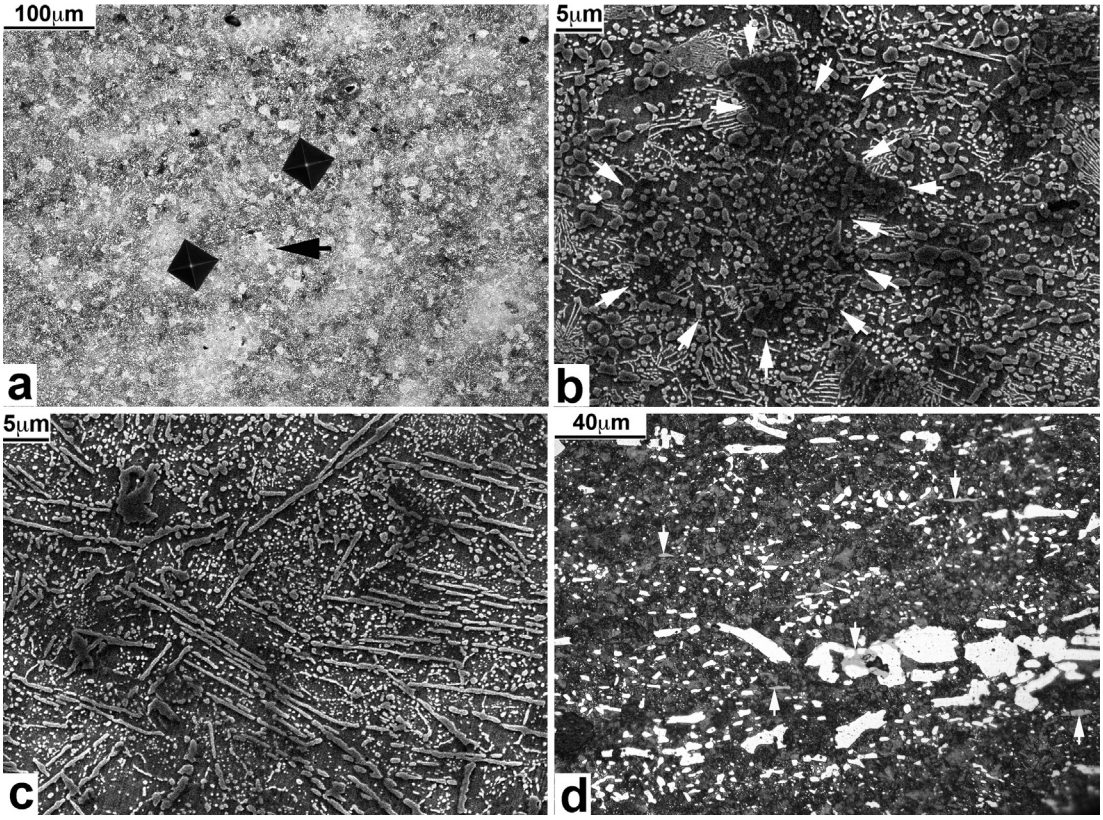

Fig. 8. Micrographs. (a) Optical micrograph showing the structure at arrow c of object #26 in Fig. 2; (b) SEI micrograph enlarging the area marked by the arrow in (a); (c) SEI micrograph showing the structure at arrow b of object #26 in Fig. 2, (d) optical micrograph showing the structure at arrow a of object #25.

farming tools re-sharpened likely in a process involving carburization. By contrast, no such difficulty would be expected if the technique, as inferred from Fig. 4d, were applied. The microstructure in Fig. 4d suggests that a steel plate was first carburized as an intermediary, which was then welded to a low carbon body. With this technique, no further treatment for carburization would have been needed throughout the lifespan of the given object, except for minor thermo–mechanical treatments for re-sharpening of the functional part. Furthermore, the ductile low carbon iron makes the adjacent steel layer less prone to brittle fracture even after quenching. In fact, the high carbon martensite in Fig. 4d remains fresh with no sign of tempering applied, as opposed to the martensite phase in Fig. 4f that was tempered. The advantage of this technique may have inspired the production and circulation of pre-carburized steel plates as product intermediaries. This would then allow the iron producers to meet varying consumer needs with fewer items, contributing to the standardization of the iron industry. Early evidence of this idea in practice may be found in the Xiongnu iron collection reported by Park et al. (2010, see #13 in Fig. 2 on page 2691). In that case, the specified rectangular rod was given a careful treatment to raise its overall carbon level to around eutectoid, i.e., 0.77%. Although no specific purpose is implied in its appearance, it may well have served as a product intermediary for use in the functional parts of tools and weapons.

The most distinct features of the third group (objects #17–24), as compared with the first two groups, are found in the use of casting as the major fabrication method and the use of high carbon alloys containing noticeable amounts of silicon, phosphorous and sulfur. They may be regarded as cast iron products. In view of their carbon level of approximately 2.0% or less, however, they may rather be referred to as ultrahigh carbon steel. Such a reduced carbon concentration implies higher melting points, and if the superheating required in casting is taken into account, temperatures of 1500 °C or above must be applied to cast such alloys. Also, considering the high temperature required for the practical reduction of silica, a key constituent in slag, the presence of silicon in all but one object in this group is another indication of high temperatures having been applied. Such a high temperature is not readily achieved in smelting without proper fuel and improved furnace construction. The presence of substantial amounts of sulfur, along with phosphorous, in all the objects under consideration suggests that the raw materials were smelted using mineral coal, generally high in sulfur (Rostoker and Bronson, 1990: 67). It was reported (Park et al., 2008) that cast iron from coal-based smelting first appeared in Mongolia during the Khitan period and brought about a significant transformation in the Mongolian iron industry. Evidently, the cast objects examined in this paper were all made of coal-smelted iron, suggesting that by the Mongol period this transition had occurred in Mongolia. It is also critical to note that sulfur in iron forms iron sulfide, as observed in Fig. 5b at arrow 1 and Fig. 6b at arrow 3. This compound melts at a relatively low temperature, 988 °C, and causes failure, commonly referred to as hot shortness, when subjected to hot working (Verhoeven, 1975: 195). The major driving force for the use of coal-smelted iron despite this serious disadvantage might be the ease with which coal, if available, is exploited. It is significant to note that the use of coal-based cast iron technology in Mongolia coincidently occurred with a rapid increase in the frequency and abundance of cast iron objects as recovered from excavations (Perlee, 1961). This episode suggests that mineral coal used in smelting made cast iron readily available by removing the long-standing obstacle to its mass production; namely, limited access to charcoal.

The primary advantage of cast iron as compared with bloomery iron is that it is suited for mass production. If this advantage is to have any practical effect, proper steel making processes involving cast iron must be available for the production of more versatile materials such as iron and steel. In principle, iron and steel can be made from cast iron by reducing the carbon level in a variety of processes where cast iron is treated in its liquid or solid state. The carbon concentration of 2.0% or less, as measured in the cast objects of the third group, however, is substantially lower than that of regular cast iron and is already in the range of ultrahigh carbon steel. It may then be predicted that the raw material supplied for these cast objects could directly be forged into iron and steel products without much treatment for further decarburization, subsequent to smelting. Fortunately, convincing evidence confirming this possibility was found in objects #21–24 in the third group and objects #25 and #26 in the fourth group. Objects #21–24 were all cast to shape, but no specific purpose is inferred from their fairly uniform and consistent appearance. Such objects have been recovered in large amounts and excavated from multiple Mongol sites separated by great distances. It seems likely, therefore, that they were produced on a large scale and widely circulated for a specific purpose. Moreover, it was previously proposed (Osawa, 2005: 45) that they were ingots for further processing. It is certain that they were not meant to be re-melted for casting, but were rather intended for thermo–mechanical treatments to be done in a solid-state.

Microstructures that can emerge from such ingots were observed in objects #25 and #26. They were severely forged and retain no structural features determined during solidification. Consequently, their probable connection with objects #21–24 is not obvious. Nevertheless, there are several factors identified in their microstructure that can serve as clues for assessing the raw materials supplied for their fabrication. First, their overall carbon concentration is much higher than is normally required for their given functional purposes. Such a high carbon level would not have been intended if low carbon iron had been supplied as a starting material. By contrast, it could have been readily obtained from materials such as those used in objects #21–24. If these ingots were subjected to forging at elevated temperatures, they would naturally take the form of flat plates with their general carbon content reduced by decarburization occurring near the surface region (Park, 2008). In this process, the large and brittle proeutectoid cementite precipitates would fragment and give rise to structures such as those illustrated in Figs. 7a and 8d. This fragmentation, if properly controlled, would promote the dissolution of carbide particles in the neighboring steel matrix and, in due time, large-scale cementite particles would disappear as can be seen in Figs. 7c and 8a. The carbon level in objects #25 and #26, still much higher than is necessary, indicates that the forging treatment was given primarily for shaping, not for the control of carbon concentration. The sulfide particles elongated along the forging planes as seen in Fig. 7b and c must have been inherited from the parent material, constituting unmistakable evidence for the connection between objects #21–24 as product intermediaries and objects #25 and #26 as finished items. This connection is also evident in the presence of the alloying elements, silicon and phosphorous, detected in both sets of objects.

The analytical results summarized in Table 1 demonstrate that the iron industry supporting Karakorum during the Mongol period was based on two different technological traditions. The first tradition, represented by objects #1–16, is characterized by the use of low carbon iron as the primary raw material and carbon control by carburization. This tradition is basically the same as that of the Xiongnu Empire (Park et al., 2010) where the smelting of bloomery iron and steel making through carburization played a key role. By contrast, the second tradition represented by objects #17–24 and objects #25 and #26 is characterized by the smelting of cast iron in the molten state and carbon control by decarburization in the solid-state. The key raw materials in the two traditions are clearly distinguished in terms of carbon concentrations, the presence of silicon and phosphorous and the chemistry of the nonmetallic inclusions, which are oxide and sulfide-based, respectively. Although cast iron objects were used in the Xiongnu communities, their use was infrequent and limited to certain Chinese-style objects. It has yet to be determined whether cast iron artefacts from the Xiongnu sites were domestically produced or imported. In any case, it is almost certain that cast iron and its relevant technologies were recognized in Mongolia at that time. Nevertheless it was not until the Khitan period that there was a notable increase in the use of cast iron. The diversity and abundance of this, as reflected in objects #17–26, suggests that the development of the Khitan period, associated with the use of fossil fuel, was carried forward to the subsequent Mongol Empire.

The impact brought about by the increased availability of cast iron, however, was evidently far from being sufficient enough to substitute cast iron for bloomery iron. Despite the advanced smelting and steel making technologies involving cast iron, the majority of the iron objects in Fig. 2 are of bloomery origin. More significantly, they comprise critical tools and weapons with superior functional properties, as is exemplified in the microstructures of objects #12 and #14. It is impressive to note that the early iron tradition established during the Xiongnu Empire continued to dominate the iron industry supporting the Mongol Empire. This fact is particularly surprising if one considers the craftsmen's quarter mentioned by William of Rubruck, which was apparently home to a Chinese community in Karakorum at the time. Evidently, the people in Mongolia still maintained their own bloomery-based iron tradition, with the cast iron-based technology serving only as a supplement primarily for large-scale casting mainly of cauldrons, farm implements (Gelegdorj et al., 2007) and guns (Erdenekhishig et al., 1995). This episode suggests that small-scale production with a low initial investment, a unique feature of bloomery technology, was still highly regarded given the nomadic life style of the people from this steppe region. The special cast ingots illustrated in objects #21–24 may then be interpreted as an effort to enhance the applicability of cast iron. It is evident that such ingots were widely circulated as a feedstock for further processing. Their contribution, however, was likely limited due to the presence of sulfide inclusions and a general lack of technological understanding in how to deal effectively with such high carbon material. The hot shortness encountered in sulfur-contaminated iron must have seriously restricted the usefulness of such objects as a feedstock for forging. Furthermore, finished items made from these intermediaries would have been prone to brittle fracture in service without proper control over the shape and distribution of carbide precipitation. The structure in Fig. 8a shows that such control was rather successful while Fig. 8d represents a failed attempt. In view of their size and shape appropriate for ready transportation, some of such special cast iron ingots may have been produced in a remote place such as China and then imported.

5. Summary and conclusion

Twenty-six iron objects recovered from Karakorum, the former capital of the Mongol Empire, were characterized in terms of smelting, steel making and thermo–mechanical treatments employed for their fabrication. The majority (sixteen) of them were forged from low carbon iron with features characteristic of bloomery products while the rest (ten) originated from cast iron containing 2.0% or less carbon and trace amounts of sulfur, silicon and phosphorous. Eight of the cast objects remain in as-cast conditions while the other two show clear evidence of substantial forging applied subsequent to casting. The bloomery-based

technology as inferred from the bloomery products examined shows no notable difference from that practiced during the Xiongnu period approximately a millennium before. The cast iron-based technology, however, made substantial progress, and a large number of cast products were used at Karakorum during the Mongol Empire for a variety of purposes. This technological progress was evidently associated with a transition initiated during the previous Khitan period in keeping with the use of coal-smelted cast iron. The transition seems to have spread rapidly and was completed by the Mongol period such that coal-based cast iron was the norm of the local cast iron industry. This fact suggests that limited access to charcoal had long been a major barrier to the availability of cast iron in Mongolia.

It is important to note, however, that at Karakorum for the Mongol period, bloomery-based technology still played a key role in the production of critical items such as tools and weapons. By contrast, the use of cast iron was limited to the manufacturing of large-scale farming tools and domestic items, which do not require a strict control of the material properties used. The circulation of certain cast items as intermediaries for making steel products should then be understood as an effort to expand the applicability of cast iron that was readily available at that time. This effort was not fully successful due to the detrimental effect of hot-shortness confronted in the forging of such coal-smelted, thereby sulfur-contaminated, cast products. Furthermore, the high carbon level in these items can cause brittle fractures unless the carbide precipitation is properly controlled during fabrication.

The traditional bloomery-based technology which dominated the iron industry of the Mongol Empire at Karakorum suggests that the Chinese style of cast iron-based technology was introduced at an extremely slow rate beginning in Xiongnu period. The nomadic life style of the Mongolian people may have been a major factor for such a slow technological evolution. Lastly, the Mongol Empire appears to have been successful in taking advantage of both bloomery-based and cast iron-based technologies to establish an effective multi-faceted iron tradition that was highly adaptable.

Acknowledgments

The authors would like to thank the Archaeological Institute of the Mongolian Academy of Sciences for their approval of sampling specimens for this study. For many helpful comments we also thank Jan Bemmann and Ernst Pohl of Bonn University and William Honeychurch at Yale University. This work was financially supported by the Korea National Research Foundation (NRF-2013R1A1A2059128).

References

Amartuvshin, Ch, Sasada, T., Eregzen, G., Üsüki, I., Ishtseren, L., 2012. Chronology of earthen burner for ceramics and ore at Khustyn Bulag Site. Stud. Archaeol. 32 (13), 213–228 (In Mongolian).

Allsen, T., 2002. Commodity and Exchange in the Mongol Empire: a Cultural History of Islamic Textiles. Cambridge University Press, Cambridge &New York.

Barfield, T.J., 2001. The shadow empires: imperial state formation along the Chinese-Nomad frontier. In: Alcock, S.E., D'Altroy, T.N., Morrison, K.D., Sinopoli, C.M. (Eds.), Empires: Perspectives from Archaeology and History. Cambridge University Press, Cambridge, pp. 10–41.

Erdenekhishig, T.B., Amarjargal, B., Bazarsuren, J., Shagdar, Kh, Mygmarsambuu, G., Davaasuren, B., Ariunbold, G., 1995. A History of Mongolian Warriors, vol. 1. Institute of Mongolian Military History, Ulaanbaatar (In Mongolian).

Fitzhugh, W., 2013. Genghis Khan: empire and legacy. In: Fitzhugh, W., Rossabi, M., Honeychurch, W. (Eds.), Genghis Khan and the Mongol Empire. Smithsonian Institution, Washington DC, pp. 23–39.

Gelegdorj, E., Chunag, A., Grodon, R.B., Park, J.S., 2007. Transitions in cast iron technology of the nomads in Mongolia. J. Archaeol. Sci. 34, 1187–1196.

Honeychurch, W., 2010. Pastoral nomadic voices: a Mongolian archaeology for the future. World Archaeol. 42 (3), 405–417.

Honeychurch, W., 2013. The nomad as state builder: historical theory and material evidence from Mongolia. J. World Prehist. 26 (4), 283–321.

Honeychurch, W., 2014. Alternative complexities: the archaeology of nomadic states. J. Archaeol. Res. 22 (4), 277–326.

Jackson, P. (Ed.), 1990. The Mission of Friar William of Rubruck: His Journey to the Court of the Great Khan Möngke 1253–1255. Hakluyt Society, London.

Kradin, N., 2002. Nomadism, evolution, and world-systems: pastoral societies in theories of historical development. J. World-Syst. Res. 8, 368–388.

Needham, J., 1980. The evolution of iron and steel technology in East and Southeast Asia. In: Wertime, T.A., Muhly, J.D. (Eds.), The Coming of the Age of Iron. Yale University Press, New Haven and London, pp. 507–541.

Osawa, M., 2005. One of the forms of iron producing in the Mongol Empire obtained from forge-related objects found at Avraga site. approach based on metallurgical study. In: Kato, Shimpei (Ed.), The Avraga Site. Preliminary Report of the Excavations of the Palace of Genghis Khan in Mongolia 2001–2004. Kokugakuin University, pp. 45–62.

Park, J.S., 2008. The key role of forging in ancient steelmaking from cast iron. Mater. Charact. 59, 647–650.

Park, J.S., Chunag, A., Gelegdorj, E., 2008. A technological transition in Mongolia evident in microstructure, chemical composition and radiocarbon age of cast iron artefacts. J. Archaeol. Sci. 35, 2465–2470.

Park, J.S., Eregzen, G., Yeruul-Erdene, Ch, 2010. Technological traditions inferred from iron artefacts of the Xiongnu Empire in Mongolia. J. Archaeol. Sci. 37, 2689–2697.

Perlee, Kh, 1959. A Study on the Khitan and the Khitan-Mongol Relationship. In: Studia Historica 1. Historical Institute of the Mongolian Academy of Sciences, Ulaanbaatar (In Mongolian).

Perlee, Kh, 1961. Ancient and Prehistoric Towns and Settlements of Mongolia. Mongolian Academy of Sciences, Ulaanbaatar (In Mongolian).

Pohl, E., 2009. The excavations in the Chinese craftsmen-quarter of Karakorum (KAR-2) between 2000 and 2005 – stratigraphy and architecture. In: Bemmann, J., Erdenebat, U., Pohl, E. (Eds.), Mongolian-German Karakorum Expedition 1. Excavations in the Craftsmen Quarter at the Main Road, Forschungen zur Archäologie Außereuropäischer Kulturen 8. Reichert, Wiesbaden, pp. 63–136.

Pohl, E., Mönkhbayar, L., Ahrens, B., et al., 2012. Production sites in Karakorum and its environment: a new archaeological project in the Orkhon Valley, Mongolia. Silk Road 10, 49–65.

Rostoker, W., Bronson, B., 1990. Pre-industrial Iron: its Technology and Ethnology. In: Archaeomaterials Monograph, vol. 1. University Museum Publications, Philadelphia Pennsylvania.

Sasada, T., Ishtseren, L., 2012. Study on the metallurgy of the Mongol Empire: metallurgical production at “Avraga Balgas”, the great palace of Genghis Khan. Stud. Archaeol. 32 (16), 268–277 (In Mongolian).

Sherby, O.D., Oyama, T., Kum, D.W., Wadsworth, J., 1985June1985. Ultrahigh carbon steels. J. Metals 50–56.

Shiraishi, N., Tsogtbaatar, B., 2009. A preliminary report on the Japanese-Mongolian joint archaeological excavation at Avraga Site: the great Ordu of Chinggis Khan. In: Bemmann, J., Parzinger, H., Pohl, E., Tseveendorzh, D. (Eds.), Current Archaeological Research in Mongolia. Papers from the First International Conference on “Archaeological Research in Mongolia” Held in Ulaanbaatar, August 19th–23rd, 2007, Bonn Contributions to Asian Archaeology, vol. 4. Vor- und Frühgeschichtliche Archäologie, Rheinische Friedrich-Wilhelms-Universität, Bonn, pp. 549–562.

Tylecote, R.F., 1962. Metallurgy in Archaeology – a Prehistory of Metallurgy in the British Isles. Edward Arnold, London.

Verhoeven, J.D., 1975. Fundamentals of Physical Metallurgy. John Wiley & Sons, New York, Chichester, Brisbane, Toronto.

Wagner, D.B., 2008. Science and civilization in China. In: Needham, Joseph (Ed.), Chemistry and Chemical Technology Part 11: Ferrous Metallurgy, vol. 5. Cambridge University Press, Cambridge.